European Journal of Radiology 111 (2019) 14–20

Contents lists available at ScienceDirect

European Journal of Radiology

journal homepage: www.elsevier.com/locate/ejrad

Reducing artifacts from total hip replacements in dual layer detector CT: Combination of virtual monoenergetic images and orthopedic metal artifact reduction

Victor Neuhaus[1,*], Nils Grosse Hokamp[1], David Zopfs, Kai Laukamp, Simon Lennartz, Nuran Abdullayev, David Maintz, Jan Borggrefe

Department of Diagnostic and Interventional Radiology, University Hospital Cologne, Cologne, Germany

ARTICLE INFO

Keywords:
Dual-energy CT
Dual-layer CT
Metal artifact reduction
Virtual monoenergetic images
Iterative metal artifact reduction

ABSTRACT

Purpose: To evaluate the reduction of artifacts caused by total hip replacements (THR) in dual-layer DECT (DLCT) provided by the combination of virtual monoenergetic images (VMI) and orthopedic metal artifact reduction (MAR).

Materials and Methods: A total of 24 consecutive patients carrying THR, who received DLCT, were included. Four different images were reconstructed from the same CT dataset: a) conventional images (CI), b) conventional images with orthopedic metal artifact reduction (CI_{MAR}) c) VMI and d) VMI combined with orthopedic metal artifact reduction (VMI_{MAR}). VMI and VMI_{MAR} were reconstructed at 140 keV, 160 keV, 180 keV and 200 keV. Attenuation (HU) and noise (SD) were measured in order to evaluate reduction of hypodense and hyperdense artifacts, evaluate reduction of image noise as well as to calculate contrast-to-noise ratios (CNR). Image quality was additionally rated with regard to: a) extent of artifact reduction and assessment of b) pelvic organs, c) bone and d) muscle adjacent to the metal implants. Statistical analysis was performed using Wilcoxon test.

Results: VMI_{MAR} at high keV, 140, 160, 180 and 200 keV, led to the greatest reduction of hypodense artifacts in comparison to plain VMI or CI_{MAR} ($p < 0.01$), while in comparison to CI hyperdense artifacts were significantly reduced in all reconstructions ($p < 0.05$). Accordingly, subjective analysis found VMI_{MAR} to be superior in reducing hypodense artifacts in comparison to VMI and CI_{MAR} ($p < 0.05$), while hyperdense artifacts were equally reduced in all reconstructions compared to CI ($p < 0.0001$). Additionally, assessment of the pelvic organs and adjacent bone was significantly improved in VMI_{MAR} in comparison to VMI and CI_{MAR} ($p < 0.05$). In contrast, muscles adjacent to the metal implants were significantly better assessable in all reconstructions compared to CI ($p < 0.01$).

Conclusion: The combination of VMI and MAR yields strongest reduction of hypo- and hyperdense artifacts caused by total hip replacements in staging DLCT in comparison to each technique by itself.

1. Introduction

The increasing prevalence of arthroplasties is a challenge for diagnostic imaging, especially in computed tomography (CT), since image quality and diagnostic accuracy of CT are impaired by artifacts caused by orthopedic metal implants [1,2].

Especially total hip replacements (THR) cause severe artifacts due to photon starvation (i.e. complete absorption of the photons of the x-ray) [3] and beam hardening (i.e. increased attenuation of the low energy photons in comparison to the high energy photons of the x-ray) [4,5]. Due to these artifacts, the evaluation of the implant itself, the implant-bone-interface and also adjacent soft tissues such as the intrapelvine organs is impaired.

Generally, artifacts caused by metal implants can be reduced using techniques based on single-energy or dual-energy CT [6–14]. Acquisition and reconstruction parameters of CT scans can be optimized in order to reduce artifacts caused by metal implants, e. g. by increasing the tube current time product as well as the tube voltage. However, the extent of artifact reduction is limited and these modifications may result in a higher radiation dose [6]. Post-processing algorithms for metal artefact reduction, based on single-energy CT, use means of iterative reconstructions and have been found capable of reducing the artifacts

* Corresponding author at: Institute of Diagnostic and Interventional Radiology, University Hospital Cologne, Kerpener Str. 62, 50937, Cologne, Germany.
E-mail address: victor-frederic.neuhaus@uk-koeln.de (V. Neuhaus).
[1] Contribute equally.

https://doi.org/10.1016/j.ejrad.2018.12.008
Received 20 August 2018; Received in revised form 5 December 2018; Accepted 6 December 2018

caused by THR to some extent [7–9,14]; however, they might introduce new artifacts adjacent as well as in between metal implants possibly leading to false positive findings in the clinical interpretation of images [14–16]. In contrast, virtual monoenergetic images (VMI) based on dual-energy CT (DECT) approximate images that would result from true monoenergetic acquisitions and are calculated as linear combinations of the high-energy and the low-energy datasets acquired in DECT [17]. The resulting virtual monoenergetic images (VMI) are capable to reduce moderate artifacts caused by metal implants at higher kiloelectronvolt levels [10–13]. However, VMI have been found to fail to significantly reduce severe artifacts caused by THR [10,11].

First results indicate a possible additive effect when combining techniques based on single-energy CT, e. g. post-processing algorithms for metal artefact reduction, and techniques based on dual-energy CT, i.e. VMI [12,18–24]. However, the combination of both techniques in dual-layer DECT (DLCT) has not been evaluated to date. Thus, the purpose of this study is to evaluate the reduction of artifacts caused by THR in routine staging dual-layer DECT (DLCT) provided by the combination of virtual monoenergetic images and orthopedic metal artifact reduction (VMI_{MAR}). For this purpose, we compared artifacts in virtual monoenergetic images, which were computed in combination with orthopedic metal artifact reduction (VMI_{MAR}) and without these algorithms (VMI) as well as in conventional images computed with orthopedic metal artifact reduction (CI_{MAR}) and without these algorithms (CI).

2. Materials and methods

This study was approved by the institutional review board and informed consent was waived due to the retrospective character. We identified 29 consecutive patients who carried uni- or bilateral total arthroplasties of the hips and received routine staging DLCT of the abdomen including the entire pelvis in portal venous contrast phase. DLCT has been conducted with clinical indications for staging of different malignancies, e. g. rectal or prostate cancer; no CT was acquired solely for the purpose of this study.

Out of the 29 identified patients five patients were excluded due to patient movement (n = 1) or due to insufficient filling of the bladder impairing calculation of the CNR (n = 4). The mean age of the 24 included patients was 71 ± 10.7 years (ranging from 42 to 89 years). Bilateral total arthroplasties of the hips were found in eight patients, while 16 patients showed unilateral total arthroplasty of the hip.

2.1. Image acquisition

All CT scans were performed using a dual-layer detector CT (IQon Spectral CT, Philips, Best, the Netherlands). Scans were conducted with a pitch of 0.671, a collimation of 64 × 0.625 mm, a rotation time of 0.33 s, dose modulation (DoseRight 3D-DOM; Philips Healthcare), and a tube voltage of 120 kVp. Contrast agent (80 ml, Accupaque 350, GE Healthcare, Chalfont St Giles) was administered via a cubital vein with a constant flow of 4.0 ml/min followed by a 30 ml saline flush using an automated injector (Medrad Stellant CT injection system, Bayer Healthcare, Leverkusen, Germany). Bolus tracking was used to start image acquisition by placing a region of interest in the abdominal aorta, using a trigger threshold of 150 HU and a start delay of 70 s.

2.2. Image reconstruction

Conventional as well as virtual monoenergetic images were reconstructed in the axial plane with a slice thickness of 2 mm and a section increment of 1 mm. Conventional and virtual monoenergetic images were computed using a dedicated reconstruction algorithm (Spectral B, level 3, Philips Healthcare), which is required since the reconstruction of spectral results is carried out in the projection domain and conventional image reconstruction algorithms cannot be utilized. However, the dedicated reconstruction algorithm (Spectral B, Philips Healthcare) contains elements of iDose [4] and IMR (Philips Healthcare). Thus, the conventional images are identical to the vendor's hybrid iterative reconstruction algorithm (iDose [4], level 3) in regard to the reduction of noise [25]. Conventional as well as virtual monoenergetic images were reconstructed either combined with or without orthopedic metal artifact reduction (O-MAR, Philips Healthcare) [26], which will be referred to as CI_{MAR} or CI and VMI_{MAR} or VMI, respectively. VMI_{MAR} and VMI were also reconstructed at different kiloelectronvolt levels (140 keV, 160 keV, 180 keV and 200 keV).

2.3. Image analysis

Quantitative and qualitative analysis was carried out using the proprietary image viewer (IntelliSpace Portal Spectral Diagnostics Suite, Philips).

For quantitative assessment, regions of interest (ROI) were placed in the same axial slice close to the metal implant, medially in the most pronounced hypodense artifact obscuring the pelvic soft tissue, laterally in the most pronounced hyperdense artifact by one radiologist (DZ) with two years of experience in reading CTs, who received a training prior to quantitative assessment (Fig. 1). Furthermore, ROIs were placed in the acetabulum, the gluteus maximus muscle, subcutaneous fat, not affected by the artifacts, as well as in the urine filled bladder (Fig. 1). ROIs were placed on CI (soft tissue window (width 360, center 60). Location and size of the ROIs (65 mm^2) were then used as a template for the other image reconstructions and thus kept constant in conventional and virtual monoenergetic images as well as across the different keV. The size of the ROIs was only adjusted to prevent inclusion of tissues not affected by the artifacts and of different attenuation, respectively. Attenuation values and standard deviation within the ROI were automatically recorded from the same ROI for CI and VMI at 140 keV, 160 keV, 180 keV and 200 keV. Attenuation values and standard deviation were used to calculate contrast-to-noise ratios (CNR) as follows: the difference of the average attenuation within the ROI placed in the bladder and the subcutaneous fat divided by the square root of the sum of the variances within those ROI [27]. In addition to these measurements the width of the most pronounced hypodense artifact obscuring the pelvic soft tissue, thus in between hip joints, located over the pelvic soft tissue, was measured.

For qualitative assessment, the extent of hypodense and hyperdense artifacts were separately assessed by two radiologists (NGH and KL) with four and three years of experience in reading CT, who received a training prior to qualitative assessment. Qualitative assessment was conducted using a five-point Likert-scale (massive artifacts = 1, pronounced artifacts = 2, moderate artifacts = 3, little artifacts = 4, no artifacts = 5). Further, the assessment of the bone and muscle adjacent to the metal implant as well as the assessment of the pelvic organs were rated (not assessable = 1, limitedly assessable = 2, moderately assessable = 3, well assessable = 4, fully assessable = 5). For qualitative assessment, modification of the window settings as well as the use of multiplanar reconstructions were allowed.

2.4. Statistical analysis

Interval scaled data are reported as mean and standard deviation, ordinal scaled data as median and range. After rejection of normal distribution by Shapiro-Wilk test, further analysis was performed using Wilcoxon test with Steel-Dwass correction for multiple comparisons. Statistical analysis was performed using JMP Software (v12, SAS Institute, Cary, USA). P-values ≤ 0.05 were considered significant.

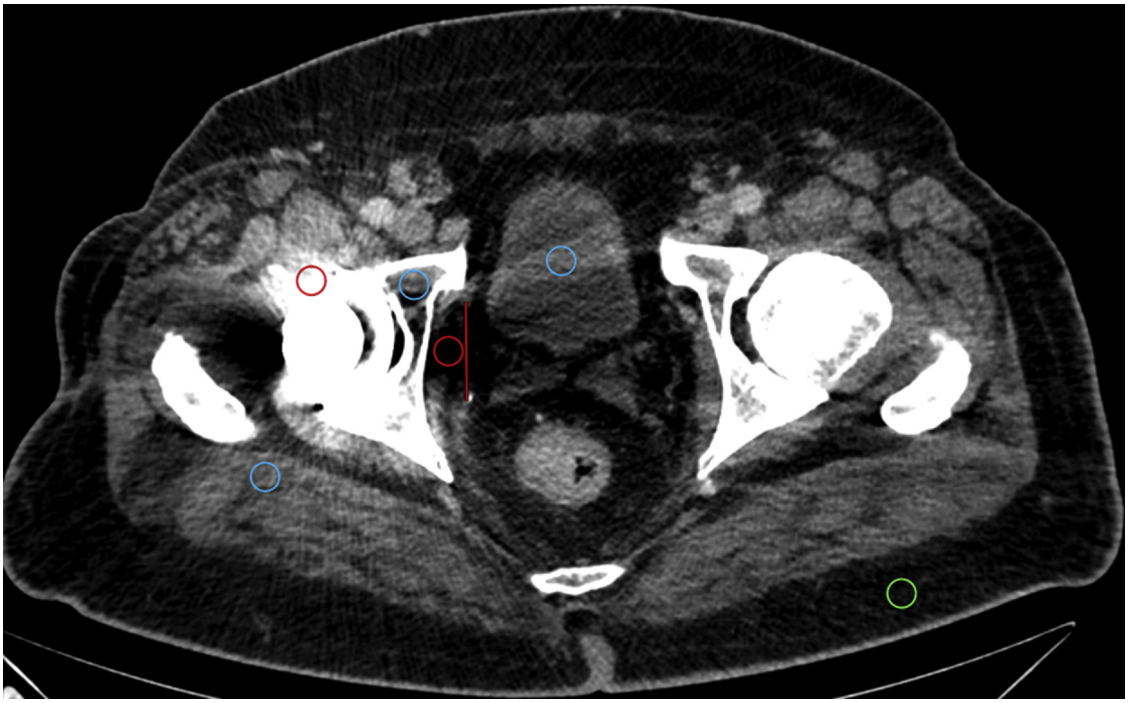

Fig. 1. Quantitative assessment of image quality, regions of interest (ROI) were placed close to the metal implant, medially in the most pronounced hypodense artifact obscuring the pelvic soft tissue as well as laterally in the most pronounced hyperdense artifact within the adjacent muscles (red ROIs). Furthermore, ROI were placed in the subcutaneous fat (green ROI), not affected by the artifacts, as well as in the adjacent bone (acetabulum) and muscle (gluteus maximus muscle) as well as the urine filled bladder (blue ROI). ROI were placed on CI (soft tissue window (width 360, center 60)) and kept constant in conventional and virtual monoenergetic images as well as across the different keV. Additionally, the width of the most pronounced hypodense artifact was measured (red line).

3. Results

3.1. Objective analysis

3.1.1. Reduction of hypodense artifacts

By definition, the measured hypodense artifacts exhibited negative HU in CI (-388.2 ± 168.5 HU; Fig. 2, Table 1). Significantly higher HU were observed in the VMI_{MAR}, e. g. at 200 keV (-66.7 ± 67.5 HU; $p < 0.0001$), as well as in CI_{MAR} (-128.1 ± 43.4 HU; $p < 0.0001$; Figs. 2 and 4, Table 1). Further, the measured HU of the hypodense artifacts were significantly higher in VMI_{MAR} at 140 keV, 160 keV, 180 keV and 200 keV in comparison to CI_{MAR} ($p < 0.05$). No significant difference was detected between the different keV levels of the VMI_{MAR} ($p > 0.5$).

The average width of the hypodense artifacts, measured in CI was 35.2 mm ± 8.6 mm and decreased to a minimum of 11 mm ± 12.6 mm in VMI_{MAR} at 200 keV ($p < 0.007$; Fig. 2, Table 1). In VMI_{MAR} at 200 keV and 180 keV the width of the hypodense artifacts was significantly smaller than in VMI and in CI_{MAR} ($p < 0.05$).

3.1.2. Hypodense artifacts caused by unilateral THR

In case of unilateral THR, the hypodense artifacts were significantly reduced in CI_{MAR} and in VMI_{MAR} ($p < 0.001$; Fig. 2). The reduction of the hypodense artifacts did not differ significantly in those reconstructions. However, the width of the hypodense artifacts was significantly reduced in VMI_{MAR} only ($p < 0.01$).

3.1.3. Hypodense artifacts caused by bilateral THR

In case of bilateral THR, the hypodense artifacts were reduced by VMI_{MAR} and CI_{MAR} only ($p < 0.05$; Fig. 2). Here, VMI_{MAR} did not yield a significant improvement in comparison to CI_{MAR}.

The width of the hypodense artifacts was noticeably reduced in VMI_{MAR} at different keV levels and in CI_{MAR}. Here the width showed strongest reduction in VMI_{MAR} at 200 keV in comparison to CI_{MAR} (Figs. 2 and 4). However, no statistical significance was detected.

3.1.4. Reduction of hyperdense artifacts

The measured hyperdense artifacts adjacent to the THR showed positive HU in CI (401.2 ± 201.3 HU), which were significantly decreased in VMI and VMI_{MAR}, e.g. at 200 keV to 149.9 ± 267.3 HU ($p < 0.02$) and 46.5 ± 62.3 HU ($p < 0.0001$, Figs. 3 and 4 , Table 1), respectively, as well as in CI_{MAR} (109.4 ± 78.3 HU; $p < 0.0001$; Fig. 3, Table 1), while there was no statistical difference detected between the above-mentioned reconstructions.

3.1.5. Hyperdense artifacts caused by unilateral THR

The hyperdense artifacts caused by unilateral THR were significantly reduced in all reconstructions compared to CI ($p < 0.05$, Fig. 3), except for VMI at 140 keV ($p = 0.05$).

3.1.6. Hyperdense artifacts caused by bilateral THR

In patients carrying bilateral THR the hyperdense artifacts were only significantly reduced in VMI_{MAR} at 140–200 keV ($p < 0.05$, Figs. 3 and Fig. 44).

3.1.7. Attenuation of surrounding tissues and pelvic organs

Attenuation within bone and muscle was found highest in CI compared to all other reconstructions, likely due to predominance of hyperattenuating artifacts ($p < 0.03$; Table 2). This also accounts for CI_{MAR} in comparison to VMI_{MAR} at high keV ($p < 0.03$).

Attenuation of the bladder was highest in CI_{MAR} (Table 2); however no significant differences were observed in comparison to the other reconstruction.

3.1.8. Image noise in surrounding tissues and pelvic organs

Image noise in the muscle and the bone adjacent to the metal implant as well as in the bladder was significantly reduced in all reconstructions in comparison to CI ($p < 0.05$; Table 1). Further,

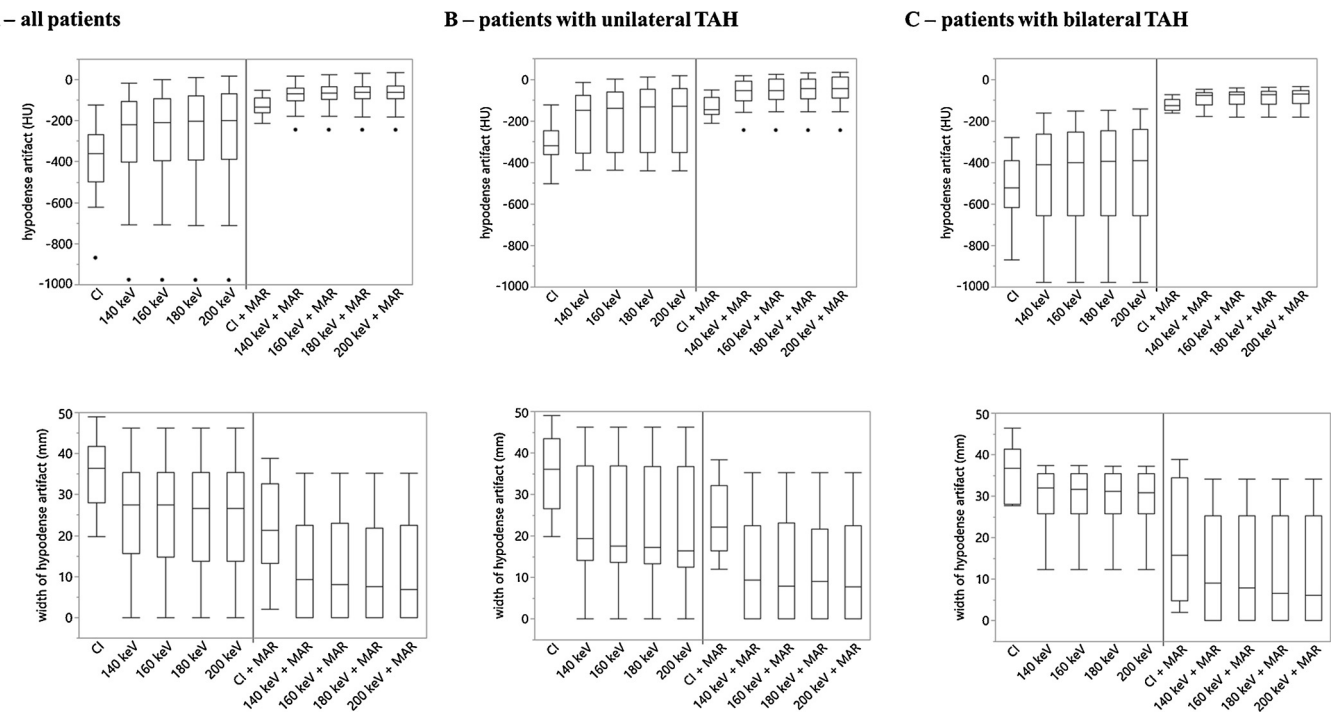

Fig. 2. Box-plots showing mean HU and width of hypodense artifacts measured in the different reconstructions in all patients (A), in patients carrying unilateral (B) and bilateral THRs (C). Vertical lines between bars indicate reconstructions not combined with MAR (left) and reconstructions combined with MAR (right) (CI, conventional images; VMI, virtual monoenergetic images; CI + MAR, conventional images combined with orthopedic metal artifact reduction algorithm; VMI + MAR, virtual monoenergetic images combined with orthopedic metal artifact reduction algorithm).

VMI_{MAR} reduced the image noise significantly stronger than CI_{MAR} regarding adjacent muscle and bladder ($p < 0.01$).

3.1.9. Contrast-to-noise ratio within surrounding tissues and pelvic organs

CNR of adjacent bone and muscle as well as within the bladder was highest in CI_{MAR} (Table 2). In regard to adjacent bone and the bladder no statistic differences were observed between different reconstructions. CNR of adjacent muscle was significantly higher in CI_{MAR} in comparison to VMI at 180 and 200 keV ($p < 0.03$) as well as significantly higher in VMI_{MAR} at 140 and 160 keV in comparison to VMI at 200 keV ($p < 0.04$).

3.2. Subjective analysis

All reconstructions visually reduced hypodense artifacts in comparison to CI ($p < 0.01$; Table 3). VMI_{MAR} at 160 keV, 180 keV and 200 keV received superior scores compared to all other reconstruction with regard to the reduction of hypodense artifacts ($p < 0.05$).

Hyperdense artifacts were rated significantly lower in all reconstructions in comparison to CI ($p < 0.0001$; Table 3), while VMI_{MAR} at 200 keV received higher scores than VMI at other keV levels ($p < 0.05$).

While all reconstructions except VMI at 140 keV improved the assessment of the pelvic organs in comparison to CI significantly ($p < 0.05$; Table 3), assessment of the pelvic organs received highest ratings in VMI_{MAR} at 200 keV and 180 keV ($p < 0.05$). Further, no

Table 1
Results of objective image analysis. Average attenuation and width of the hypo- and hyperdense artifacst as well as noise in the surrounding tissues and pelvic orangs (SD, standard deviation; CI, conventional images; VMI, virtual monoenergetic images; CI_{MAR}, conventional images combined with orthopedic metal artifact reduction algorithm; VMI_{MAR}, virtual monoenergetic images combined with orthopedic metal artifact reduction algorithm).

	artifacts			noise in surrounding tissues and pelvic organs			
	hypodense		hyperdense	bone	muscle	bladder	subcutaneous fat
	attenuation	width	attenuation	SD	SD	SD	SD
CI	−388.2 ± 168.0	35.2 ± 8.6	401.2 ± 201.3	89.0 ± 43.0	34.0 ± 18.2	26.8 ± 13.3	17.3 ± 3.6
VMI							
140 keV	−282.7 ± 228.0	25.1 ± 13	187.6 ± 244.1	62.1 ± 49.4	27.2 ± 22.1	19.8 ± 10.5	12.4 ± 2.5
160 keV	−274.0 ± 233.0	24.7 ± 13.2	176.3 ± 251.2	60.5 ± 49.7	27.7 ± 22.0	19.4 ± 10.4	12.3 ± 2.4
180 keV	−268.0 ± 236.2	24.5 ± 13.2	157.9 ± 262.1	60.1 ± 49.6	27.9 ± 22.1	19.4 ± 10.2	12.2 ± 2.4
200 keV	−264.0 ± 238.2	24.3 ± 13.3	150.0 ± 267.3	59.6 ± 49.8	28.1 ± 22.1	19.4 ± 10.1	12.2 ± 2.4
CI_{MAR}	−128.1 ± 43.4	22.5 ± 11.2	109.4 ± 78.3	49.2 ± 24.0	21.7 ± 4.3	19.7 ± 4.2	14.1 ± 2.9
VMI_{MAR}							
140 keV	−75.7 ± 63.3	12.0 ± 12.3	56.2 ± 61.8	35.7 ± 21.9	15.5 ± 3.1	15.0 ± 3.5	10.6 ± 2.3
160 keV	−71.4 ± 65.3	11.3 ± 12.5	51.6 ± 61.9	35.0 ± 21.9	15.3 ± 3.1	14.9 ± 3.5	10.6 ± 2.3
180 keV	−68.6 ± 66.6	11.1 ± 12.6	48.6 ± 62.1	34.5 ± 21.9	15.2 ± 3.1	14.8 ± 3.4	10.5 ± 2.2
200 keV	−66.7 ± 67.5	11.0 ± 12.6	46.5 ± 62.3	34.2 ± 21.8	15.1 ± 3.1	14.8 ± 3.4	10.5 ± 2.3

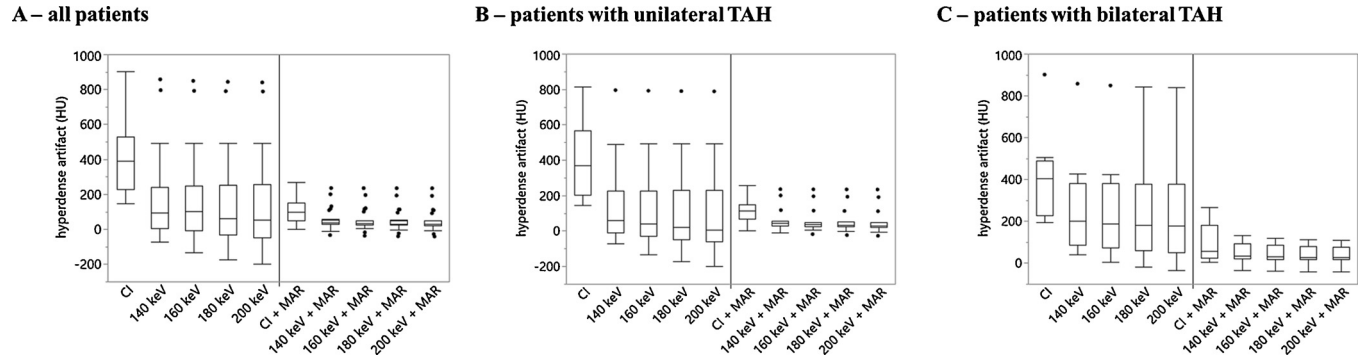

Fig. 3. Box-plots showing mean HU of hyperdense artifacts in the different reconstructions in all patients (A) and patients carrying bilateral total arthroplasties of the hips (B) (CI, conventional images; VMI, virtual monoenergetic images; CI + MAR, conventional images combined with orthopedic metal artifact reduction algorithm; VMI + MAR, virtual monoenergetic images combined with orthopedic metal artifact reduction algorithm).

significant difference was detected between VMI_{MAR} at 200 keV and 180 keV.

In comparison to CI, the assessment of the bone adjacent to the metal implant was improved in all reconstructions ($p < 0.001$; Table 3); however, VMI_{MAR} at 180 and 200 keV yielded further improvement as compared to CI_{MAR} ($p < 0.01$).

Assessment of the muscle adjacent to the metal implant was found to be significantly better in all reconstructions in comparison to CI ($p < 0.01$; Table 3). Here, we found no significant difference between any VMI, CI_{MAR} or VMI_{MAR}.

4. Discussion

The presented study evaluates the reduction of artifacts caused by total hip replacement (THR) in staging DLCT provided by the combination of virtual monoenergetic images combined with a metal artifact reduction algorithm.

Previous studies reported a reduction of artifacts caused by THR by using plain VMI without additional dedicated metal artifact reduction algorithms [7,8]. However, in these studies VMI failed to reduce severe artifacts caused by THR, especially in implants made of steel and/or bilateral implants. The latter cause severe photon starvation, resulting mostly in hypodense streaks. Authors argued, that especially hypodense artifacts were not addressed successfully, while hyperdense artifacts were improved significantly as high kiloelectronvolt levels primarily reduce beam hardening because of the physical characteristics of the virtual monoenergetic x-rays [8,10,11,18,25,28,29].

In contrast, studies investigating metal artifact reduction by means of dedicated image reconstruction algorithms reported a sufficient reduction of hypodense artifacts, while hyperdense artifacts remained unaltered [7,8,12,26,30]. Notably, image noise is high in images reconstructed with orthopedic metal artifact reduction and new artifacts may be induced [12,26].

Some studies directly compared VMI and dedicated image reconstruction algorithms [12,22]. They found that either technique allows for artifact reduction, but has different advantages over the other. Laukamp et al. found that in presence of arthroplasties of the hip, VMI were especially helpful for assessment of the metal-bone-interface and for reduction of hyperdense artifacts, while iterative metal artifact reduction improved the evaluation of soft tissue and reduced hypodense artifacts [22]. Yet, either technique for itself was unable to reduce artifacts entirely.

In accordance with these studies, we observed a comparable reduction of the hyperdense artifacts adjacent to unilateral THRs, mainly caused by beam hardening, in VMI and all other reconstructions; leading to an improved assessment of the bone and muscle adjacent to the THR in the subjective reading. However, in case of bilateral THR, VMI_{MAR} reduced the hyperdense artifacts adjacent to the metal implants significantly stronger, while VMI alone failed to reduce such strong artifacts.

Even though we found a significant reduction of the hypodense artifacts obscuring the pelvic organs as well as an improved assessment

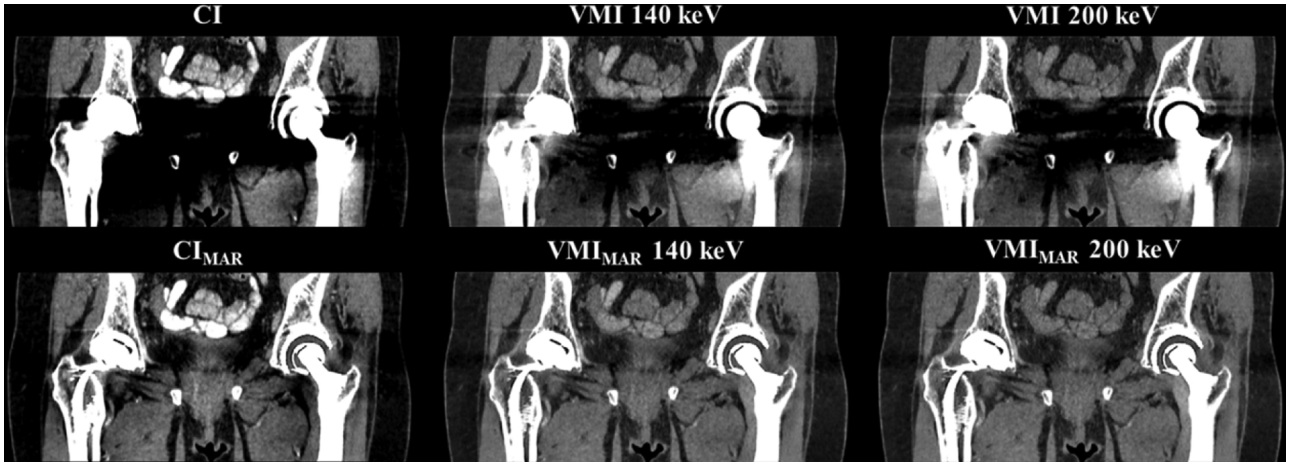

Fig. 4. Coronal images of a patient showing bilateral THRs (abdominal window with a center of 60 HU and a width of 360 HU). Images were reconstructed as CI, as VMI at 140 keV and 200 keV, as CI_{MAR} and VMI_{MAR} at 140 keV and 200 keV (CI indicates conventional images; VMI, virtual monoenergetic images; CI_{MAR}, conventional images combined with orthopedic metal artifact reduction algorithm; VMI_{MAR}, virtual monoenergetic images combined with orthopedic metal artifact reduction algorithm). The severe artifacts make diagnostic assessment of pelvic organs virtually impossible. while CI_{MAR} and VMI clearly reduce these; the combination of both techniques (VMI_{MAR}) allows for a nearly artifact free image.

Table 2
Results of objective image analysis. Average attenuation and CNR of surrounding tissues and pelvic orangs (CI, conventional images; VMI, virtual monoenergetic images; CI_{MAR}, conventional images combined with orthopedic metal artifact reduction algorithm; VMI_{MAR}, virtual monoenergetic images combined with orthopedic metal artifact reduction algorithm).

	attenuation of surrounding tissues and pelvic organs				CNR of surrounding tissues and pelvic organgs		
	bone	muscle	bladder	subcutaneous fat	bone	muscle	bladder
CI	263.0 ± 114.7	203.3 ± 86.7	17.1 ± 43.4	−92.9 ± 33.1	4.5 ± 1.7	13.2 ± 5.7	3.6 ± 1.6
VMI							
140 keV	135.1 ± 103.4	92.0 ± 109.2	17.2 ± 37.6	−66.3 ± 21.4	3.7 ± 2.0	9.8 ± 6.4	3.9 ± 2.2
160 keV	128.9 ± 104.1	87.5 ± 112.1	16.5 ± 38.0	−66.6 ± 23.0	3.7 ± 2.1	8.5 ± 5.8	3.9 ± 2.2
180 keV	116.7 ± 108.4	78.4 ± 115.1	17.5 ± 37.4	−64.1 ± 20.1	3.3 ± 2.1	7.7 ± 5.7	3.8 ± 2.2
200 keV	112.0 ± 109.9	74.7 ± 116.8	17.7 ± 37.3	−63.5 ± 19.8	3.3 ± 2.1	7.3 ± 5.6	3.8 ± 2.2
CI_{MAR}	128.6 ± 121.4	114.1 ± 38.7	21.5 ± 28.2	−96.0 ± 23.1	4.9 ± 2.7	17.6 ± 16.6	5.0 ± 1.4
VMI_{MAR}							
140 keV	59.2 ± 70.1	57.2 ± 30.4	18.8 ± 23.4	−67.4 ± 16.3	3.9 ± 2.0	14.0 ± 7.3	4.8 ± 1.5
160 keV	53.2 ± 67.4	53.0 ± 31.5	18.6 ± 23.2	−66.0 ± 15.8	3.7 ± 1.9	13.8 ± 7.0	4.7 ± 1.5
180 keV	49.4 ± 65.8	50.3 ± 32.3	18.5 ± 23.0	−651 ± 15.5	3.6 ± 1.8	13.5 ± 7.1	4.7 ± 1.5
200 keV	46.7 ± 64.7	48.4 ± 32.9	18.4 ± 22.9	−64.4 ± 15.3	3.5 ± 1.8	13.2 ± 7.0	4.7 ± 1.5

Table 3
Results of subjective image analysis. Median ratings of hypodense and hyperdens artifacts artifacts as well as of the assessment of bone and muscle adjacent to the metal implant and the intrapelvine organs are reported (CI indicates conventional images; VMI, virtual monoenergetic images; CI_{MAR}, conventional images combined with metal artifact reduction algorithm; VMI_{MAR}, virtual monoenergetic images combined with metal artifact reduction algorithm).

scale	reduction of artifacts		assessment of surrounding tissues		
1	massive artifacts		not assessable		
2	severe artifacts		impaired assessable		
3	moderate artifacts		moderatly assessable		
4	minimal artifacts		well assessable		
5	no artifacts		fully assessable		
	hypodense	hyperdense	adjacent bone	adjacent muscle	pelvic organs
CI	2 (1-3)	2 (1-3)	2 (1-3)	2 (1-3)	1 (1-3)
VMI					
140 keV	3 (1-4)	3 (1-5)	3 (1-5)	3 (1-4)	2 (1-4)
160 keV	3 (1-5)	3 (1-5)	3 (1-5)	3 (1-4)	2 (1-4)
180 keV	3 (1-5)	3 (1-5)	3 (1-5)	3 (1-5)	2 (1-4)
200 keV	3 (1-5)	3 (1-5)	3 (1-5)	3 (1-5)	2 (1-4)
CI_{MAR}	4 (2-5)	4 (2-5)	3 (2-5)	3 (2-5)	3 (2-5)
VMI_{MAR}					
140 keV	4 (2-5)	4 (2-5)	4 (3-5)	3 (2-5)	3 (2-5)
160 keV	4 (1-5)	4 (2-5)	4 (3-5)	3 (2-5)	3 (1-5)
180 keV	4 (1-5)	4 (2-5)	4 (3-5)	3 (2-5)	3 (1-5)
200 keV	4 (1-5)	4 (3-5)	4 (3-5)	4 (2-5)	3 (1-5)

of the pelvic organs in CI_{MAR}; VMI_{MAR} further reduced these hypodense artifacts, whether unilateral or bilateral THR were present. Additionally, image quality in CI_{MAR} decreased due to image noise, which was found to be lower in VMI_{MAR} in comparison to CI_{MAR}.

Few other previous studies investigated reduction of artifacts caused by orthopedic metal implants, especially THR, by combining VMI and iterative metal artifact reduction [19–21,24]. In contrast to our study, where a dual-layer detector dual-energy CT was used to acquire the raw data, fast-kVp-switching or dual x-ray sources were used as the technical approach to dual-energy CT in those studies. Both are fundamentally different approaches to dual-energy CT in contrast to DLCT, since the latter is detector based, while the former are tube-based. The detector based approach allows projection data-based decomposition since high- and low-energy projection data are fully matched, while the tube-based approaches perform either projection data-based decomposition after temporal and angular interpolation or image-based decomposition [31,32]. Reconstruction of virtual monoenergetic images from fully matched projection data allows for superior beam hardening correction as well as cancelation of anticorrelated noise in photoelectric and Compton scatter images [33–35]. The fully matched projection data further facilitate combination of VMI and MAR-techniques [26].

It is well known that both, VMI at high keV as well as orthopedic metal artifact reduction may each induce new artifacts, which can also be found in VMI_{MAR} [8,15–17,26]. Because of that, CI should be interpreted supplemented by VMI_{MAR} simultaneously in order avoid misinterpretation of images since the earlier represents the standard of care. As the keV-level can be adjusted while reading the images, this should be preferred over preset reconstructions at high keV, as newly introduced artifacts at high keV can be unmasked as such by adjusting the kiloelectronvolt level [8].

Previous studies recommended an adjustment of keV-level while reading the images in order to achieve optimal image quality, not only in regard to reduction of the artifacts, but also in regard to soft tissue contrast [10,13,36]. This is substantiated by the results of our objective and subjective analyses, which showed significant differences between VMI_{MAR} reconstructed at different keV in regard to reduction of hypodense artifacts obscuring the pelvic organs as well as the assessment of the pelvic organs in the subjective analysis. However, beyond these advantages no significant differences in artifact reduction for VMI_{MAR} were detected between higher keV (140 keV–200 keV). Furthermore, we measured decreasing CNR in VMI_{MAR} at increasing keV, which can be explained by the decrease in soft tissue' attenuation at increased keV. The decreased soft tissue contrast is a disadvantage of VMI_{MAR} at high keV. However, the loss of soft tissue contrast has to be accepted in order to allow assessment of intrapelvic organs and adjacent soft tissue in the presence of obscuring artifacts. In case of uni- or bilateral total arthroplasties of the hips we suggest adjusting keV, ranging from 140 keV to 200 keV, while reading VMI_{MAR} in order to yield best possible artifact reduction while maintaining contrast of pelvic organs and avoiding newly introduced artifacts. Alternatively, CI_{MAR} could be considered, when aiming for higher soft tissue contrast in comparison to VMI_{MAR}. However, image noise is higher and artifact reduction less potent in CI_{MAR} in comparison to VMI_{MAR}.

Some limitations of the presented study need to be mentioned: First, we did not investigate the impact of the metal alloy, size or shape of the total arthroplasties of the hips on metal artifact reduction, which reflects the clinical setting in which the alloy of the implant is commonly not known to the radiologist. Further, we did not investigate a potential benefit of an image acquisition with 140 kVp, which has been suggested by previous studies [11]. Even though other sophisticated approaches to measuring the extent of artifacts caused by metal implants have been used by previous studies, we solely measured attenuation and standard deviation in order to assess the extent of the artifacts substantiated by a detailed subjective assessment [8,25]. Especially the measurement of the standard deviation, referred to as noise, is affected by various

factors, e.g. scan parameters or anatomical region examined. Thus, in order to ensure a minimal comparability between the different reconstructions we kept the denoising level constant.

While in moderate artifacts resulting from single screws or orthopedic plates, the isolated use of either MAR or VMI likely yields sufficient artifact reduction, the application of either VMI or MAR separately frequently fails to reduce severe artifacts induced by either unilateral or bilateral THRs. We demonstrated, that the combination of VMI and MAR yields the strongest decrease of artifacts induced by THRs in staging DLCT in comparison to each technique separately. As the combination of both methods merges their strengths, they should be used for image interpretation, especially in presence of severe artifacts as caused by bilateral THR.

Conflicts of interest

The authors of this manuscript declare relationships with the following companies: Jan Borggrefe and David Maintz received speaker honoraria from Philips.

References

[1] L.M. Fayad, A. Patra, E.K. Fishman, Value of 3D CT in defining skeletal complications of orthopedic hardware in the postoperative patient, AJR Am. J. Roentgenol. 193 (4) October) (2009) 1155–1163.

[2] T.D. Roth, N.A. Maertz, J.A. Parr, et al., CT of the hip prosthesis: appearance of components, fixation, and complications, Radiographics 32 (4) July-August) (2012) 1089–1107.

[3] I. Mori, Y. Machida, M. Osanai, K. Iinuma, Photon starvation artifacts of X-ray CT: their true cause and a solution, Radiol. Phys. Technol. 6 (1) January) (2013) 130–141.

[4] R.A. Brooks, G. Di Chiro, Beam hardening in x-ray reconstructive tomography, Phys. Med. Biol. 21 (3) May) (1976) 390–398.

[5] L.M. Zatz, R.E. Alvarez, An inaccuracy in computed tomography: the energy dependence of CT values, Radiology 124 (July (1)) (1977) 91–97.

[6] M.J. Lee, S. Kim, S.A. Lee, et al., Overcoming artifacts from metallic orthopedic implants at high-field-strength MR imaging and multi-detector CT, Radiographics 27 (3) May-June) (2007) 791–803.

[7] R.H. Wellenberg, M.F. Boomsma, J.A. van Osch, et al., Computed tomography imaging of a hip prosthesis using iterative model-based reconstruction and orthopaedic metal artefact reduction: a quantitative analysis, J. Comput. Assist. Tomogr. 40 (6) November/December) (2016) 971–978.

[8] K. Higashigaito, F. Angst, V.M. Runge, et al., Metal artifact reduction in pelvic computed tomography with hip prostheses: comparison of virtual monoenergetic extrapolations from dual-energy computed tomography and an iterative metal artifact reduction algorithm in a phantom study, Invest. Radiol. 50 (12) December) (2015) 828–834.

[9] J. Aissa, J. Boos, C. Schleich, et al., Metal artifact reduction in computed tomography after deep brain stimulation electrode placement using iterative reconstructions, Invest. Radiol. 52 (1) January) (2017) 18–22.

[10] V. Neuhaus, N. Große Hokamp, N. Abdullayev, et al., Metal artifact reduction by dual-layer computed tomography using virtual monoenergetic images, Eur. J. Radiol. 93 (August) (2017) 143–148.

[11] R.H. Wellenberg, M.F. Boomsma, J.A. van Osch, et al., Quantifying metal artefact reduction using virtual monochromatic dual-layer detector spectral CT imaging in unilateral and bilateral total hip prostheses, Eur. J. Radiol. 88 (March) (2017) 61–70.

[12] N. Große Hokamp, V. Neuhaus, N. Abdullayev, et al., Reduction of artifacts caused by orthopedic hardware in the spine in spectral detector CT examinations using virtual monoenergetic image reconstructions and metal-artifact-reduction algorithms, Skeletal Radiol. (September) (2017).

[13] R. Guggenberger, S. Winklhofer, G. Osterhoff, et al., Metallic artefact reduction with monoenergetic dual-energy CT: systematic ex vivo evaluation of posterior spinal fusion implants from various vendors and different spine levels, Eur. Radiol. 22 (11) November) (2012) 2357–2364.

[14] F. Morsbach, S. Bickelhaupt, G.A. Wanner, A. Krauss, B. Schmidt, H. Alkadhi, Reduction of metal artifacts from hip prostheses on CT images of the pelvis: value of iterative reconstructions, Radiology 268 (1) July) (2013) 237–244.

[15] L. Yu, H. Li, J. Mueller, et al., Metal artifact reduction from reformatted projections for hip prostheses in multislice helical computed tomography: techniques and initial clinical results, Invest. Radiol. 44 (11) November) (2009) 691-6.15.

[16] O. Watzke, W.A. Kalender, A pragmatic approach to metal artifact reduction in CT: merging of metal artifact reduced images, Eur. Radiol. 14 (5) May) (2004) 849–856.

[17] C.H. McCollough, S. Leng, L. Yu, J.G. Fletcher, Dual- and multi-energy CT: principles, technical approaches, and clinical applications, Radiology 276 (3) September) (2015) 637–653.

[18] Y.H. Lee, K.K. Park, H.T. Song, S. Kim, J.S. Suh, Metal artefact reduction in gemstone spectral imaging dual-energy CT with and without metal artefact reduction software, Eur. Radiol. 22 (6) June) (2012) 1331–1340.

[19] D. Yue, C. Fan Rong, C. Ning, et al., Reduction of metal artifacts from unilateral hip arthroplasty on dual-energy CT with metal artifact reduction software, Acta Radiol. (January) (2017) 284185117731475.

[20] K.M. Andersson, P. Nowik, J. Persliden, P. Thunberg, E. Norrman, Metal artefact reduction in CT imaging of hip prostheses—an evaluation of commercial techniques provided by four vendors, Br. J. Radiol. 88 (1052) August) (2015) 20140473.

[21] S.C. Han, Y.E. Chung, Y.H. Lee, K.K. Park, M.J. Kim, K.W. Kim, Metal artifact reduction software used with abdominopelvic dual-energy CT of patients with metal hip prostheses: assessment of image quality and clinical feasibility, AJR Am. J. Roentgenol. 203 (4) October) (2014) 788–795.

[22] K.R. Laukamp, S. Lennartz, V.F. Neuhaus, et al., CT metal artifacts in patients with total hip replacements: for artifact reduction monoenergetic reconstructions and post-processing algorithms are both efficient but not similar, Eur. Radiol. (May) (2018).

[23] S. Winklhofer, R. Hinzpeter, D. Stocker, et al., Combining monoenergetic extrapolations from dual-energy CT with iterative reconstructions: reduction of coil and clip artifacts from intracranial aneurysm therapy, Neuroradiology 60 (3) March) (2018) 281–291.

[24] M.N. Bongers, C. Schabel, C. Thomas, et al., Comparison and combination of dual-energy- and iterative-based metal artefact reduction on hip prosthesis and dental implants, PLoS One 10 (11) November) (2015) e0143584.

[25] N. Große Hokamp, A.J. Höink, J. Doerner, et al., Assessment of arterially hyperenhancing liver lesions using virtual monoenergetic images from spectral detector CT: phantom and patient experience, Abdom. Radiol. (November) (2017).

[26] N. Große Hokamp, A. Hellerbach, A. Gierich, et al., Reduction of artifacts caused by deep brain stimulating electrodes in cranial computed tomography imaging by means of virtual monoenergetic images, metal artifact reduction algorithms, and their combination, Invest. Radiol. (March) (2018).

[27] S.R. Pomerantz, S. Kamalian, D. Zhang, et al., Virtual monochromatic reconstruction of dual-energy unenhanced head CT at 65-75 keV maximizes image quality compared with conventional polychromatic CT, Radiology 266 (1) January) (2013) 318–325.

[28] M. Lewis, K. Reid, A.P. Toms, Reducing the effects of metal artefact using high keV monoenergetic reconstruction of dual energy CT (DECT) in hip replacements, Skeletal Radiol. 42 (2) Febuary) (2013) 275–282.

[29] N. Große Hokamp, K.R. Laukamp, S. Lennartz, et al., Artifact reduction from dental implants using virtual monoenergetic reconstructions from novel Spectral Detector CT, Eur. J. Radiol. 104 (July) (2018) 136–142.

[30] R.H. Wellenberg, M.F. Boomsma, J.A. van Osch, et al., Low-dose CT imaging of a total hip arthroplasty phantom using model-based iterative reconstruction and orthopedic metal artifact reduction, Skeletal Radiol. 46 (5) May) (2017) 623–632.

[31] C. Maass, M. Baer, M. Kachelriess, Image-based dual energy CT using optimized precorrection functions: a practical new approach of material decomposition in image domain, Med. Phys. 36 (8) August) (2009) 3818–3829.

[32] L.A. Lehmann, R.E. Alvarez, A. Macovski, et al., Generalized image combinations in dual KVP digital radiography, Med. Phys. 8 (5) Septemebr-October) (1981) 659–667.

[33] X. Dong, T. Niu, L. Zhu, Combined iterative reconstruction and image-domain decomposition for dual energy CT using total-variation regularization, Med. Phys. 41 (5) May) (2014) 051909.

[34] X. Zhao, J.J. Hu, Y.S. Zhao, H.T. Zhang, P. Zhang, Iterative dual energy material decomposition from spatial mismatched raw data sets, J. Xray Sci. Technol. 22 (6) (2014) 745–762.

[35] W.A. Kalender, E. Klotz, L. Kostaridou, An algorithm for noise suppression in dual energy CT material density images, IEEE Trans. Med. Imaging 7 (3) (1988) 218–224.

[36] F. Bamberg, A. Dierks, K. Nikolaou, M.F. Reiser, C.R. Becker, T.R. Johnson, Metal artifact reduction by dual energy computed tomography using monoenergetic extrapolation, Eur. Radiol. 21 (7) July) (2011) 1424–1429.